

Article

A Novel Ferrocene-Linked Thionine as a Dual Redox Mediator for the Electrochemical Detection of Dopamine and Hydrogen Peroxide

Manikandan Palinci Nagarajan ^{1,2}, Manikandan Ramalingam ¹, Ilakeya Subbiah Arivuthilagam ¹, Vishwa Paramaguru ¹, Md. Mahbubur Rahman ³ , Jongdeok Park ¹, Francis Kwaku Asiam ¹, Byungjik Lee ¹, Kwang Pyo Kim ^{2,*}  and Jae-Joon Lee ^{1,*} 

- ¹ Research Center for Photoenergy Harvesting & Conversion Technology (phct), Department of Energy & Materials Engineering, Dongguk University, 26 Phil-dong, 3-ga, Jung-gu, Seoul 04620, Republic of Korea
- ² Department of Applied Chemistry, Kyung Hee University, 1732 Deokyoung-daero, Giheung-gu, Yongin-si 17104, Republic of Korea
- ³ Department of Energy Materials Science and Engineering, Konkuk University, Chungju 27478, Republic of Korea; mahbub1982@kku.ac.kr
- * Correspondence: kimkp@khu.ac.kr (K.P.K.); jjlee@dongguk.edu (J.-J.L.)

Abstract: We introduce a novel dual redox mediator synthesized by covalently linking ferrocene dicarboxylic acid (FcDA) and thionine (TH) onto a pre-treated glassy carbon electrode. This unique structure significantly enhances the electro-oxidation of dopamine (DA) and the reduction of hydrogen peroxide (H₂O₂), offering a sensitive detection method for both analytes. The electrode exhibits exceptional sensitivity, selectivity, and stability, demonstrating potential for practical applications in biosensing. It facilitates rapid electron transfer between the analyte and the electrode surface, detecting H₂O₂ concentrations ranging from 1.5 to 60 μM with a limit of detection (LoD) of 0.49 μM and DA concentrations from 0.3 to 230 μM with an LoD of 0.07 μM. The electrode's performance was validated through real-sample analyses, yielding satisfactory results.



Citation: Palinci Nagarajan, M.; Ramalingam, M.; Subbiah Arivuthilagam, I.; Paramaguru, V.; Rahman, M.M.; Park, J.; Asiam, F.K.; Lee, B.; Kim, K.P.; Lee, J.-J. A Novel Ferrocene-Linked Thionine as a Dual Redox Mediator for the Electrochemical Detection of Dopamine and Hydrogen Peroxide. *Biosensors* **2024**, *14*, 448. <https://doi.org/10.3390/bios14090448>

Received: 13 May 2024

Revised: 14 September 2024

Accepted: 16 September 2024

Published: 19 September 2024



Copyright: © 2024 by the authors. Licensee MDPI, Basel, Switzerland. This article is an open access article distributed under the terms and conditions of the Creative Commons Attribution (CC BY) license (<https://creativecommons.org/licenses/by/4.0/>).

Keywords: redox mediator; electro-oxidation; limit of detection; ferrocene; thionine

1. Introduction

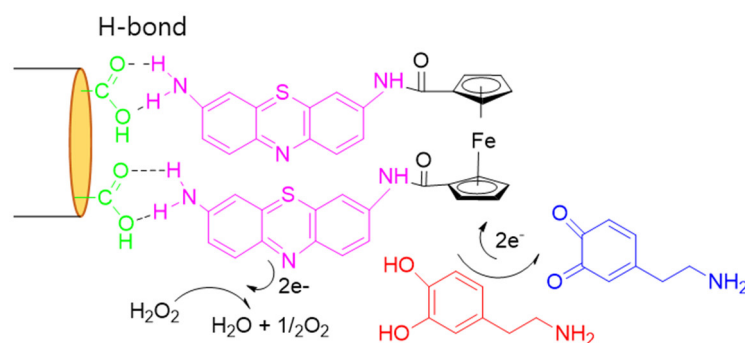
The advancement of modern analytical techniques for human health management is driven by the need to develop sustainable, reliable, and user-friendly systems for monitoring analytes in various matrices, including environmental samples, food commodities, and biological fluids [1,2]. These techniques emphasize using environmentally friendly materials and reduced reagent quantities to minimize chemical waste production.

Hydrogen peroxide (H₂O₂) is not only industrially significant but also a well-known byproduct of numerous enzymatic reactions, making its accurate quantification critical in food industries, environmental monitoring, and clinical applications [3]. As a typical reactive oxygen species, H₂O₂ can induce oxidative stress damage to cells, including neurons. The brain, with its high oxygen consumption, elevated polyunsaturated fatty acid content, and relatively low antioxidant defenses, is particularly susceptible to oxidative stress. Evidence suggests that oxidative stress may play a role in neurodegenerative disorders characterized by the loss of dopamine (DA)-producing neurons [4]. Abnormal DA levels are linked to diseases such as Parkinson's, Alzheimer's, senile dementia, and schizophrenia [5,6]. Understanding the relevance or interplay between DA and oxidative stress levels correlated with H₂O₂ levels is of significant interest [7].

Direct electrochemical detection of DA [8–16] and H₂O₂ [17–23] is well-known but typically requires sophisticated electrode design for optimization, stability, and reproducibility over a wide concentration range. This is often achieved using nanomaterials, including

conducting polymers [24,25], graphene [26–29], and redox mediators [30–34]. Early detection of DA and nitrophenol utilizing thionine (TH) as a redox mediator immobilized on glassy carbon (GC) electrodes has been reported [35–38]. Recent studies have highlighted the use of bi-mediators capable of detecting dual analytes. The complex form of nickel hexacyanoferrate and TH on GC electrodes were used for the oxidation of gallic acid and reduction of H_2O_2 [12,39], respectively, while the concept of bi- or dual-mediators for electrochemical sensors has been rarely explored.

In this study, we developed a novel electrode with a complex dual redox mediator consisting of ferrocene dicarboxylic acid (FcDA) directly linked to a TH unit. The dual mediator was synthesized by covalently linking FcDA and TH, followed by immobilization onto a pre-treated GC surface via hydrogen bonding interactions, resulting in the formation of **GC/TH–FcDA** for electrochemical sensor applications, as shown in Scheme 1. We investigated the electrochemical behavior of **GC/TH–FcDA** for the electrocatalytic detection of both DA and H_2O_2 by each electrochemically active moiety of FcDA and TH over a wide potential range at a single electrode. **GC/TH–FcDA** exhibited stable and reproducible sensing capabilities for dual analytes and can be extended for simultaneous detection of multiple analytes through simple electrode design.



Scheme 1. Electrochemical oxidation of DA and reduction of H_2O_2 on **GC/TH–FcDA**.

2. Materials and Methods

2.1. Reagents and Materials

All reagents used in this study were of analytical grade and purchased from Sigma-Aldrich (St. Louis, MO, USA) without further purification. Double-distilled water (18.2 $\text{M}\Omega\cdot\text{cm}$), obtained from a Millipore Milli-Q bio cell A10 water purification system (Merck, Darmstadt, Germany), was employed throughout the experiments. TH, FcDA, N-ethyl-N'-(3-dimethylaminopropyl)-carbodiimide hydrochloride (EDC.HCl), hydroxybenzotriazole (HOBT), DA, ascorbic acid (AA), uric acid (UA), disodium hydrogen phosphate, sodium dihydrogen phosphate, and H_2O_2 were used as received. A phosphate-buffer solution (PBS, 0.1 M, pH 7) was prepared by mixing aqueous solutions of disodium hydrogen phosphate and sodium dihydrogen phosphate. All electrochemical measurements were conducted at ambient temperature. Before measurements, the electrolyte was purged with inert nitrogen gas for 5 min to eliminate active oxygen interference.

2.2. Instrumentation

Electrochemical experiments were conducted using a CHI-430A potentiostat (CH Instruments, Austin, TX, USA) with a standard three-electrode setup. The reference and auxiliary electrodes consisted of an Ag/AgCl electrode saturated with KCl and a platinum wire. The working electrodes were GC electrodes with a diameter of 3 mm, modified with TH-FcDA to obtain **GC/TH–FcDA**. Fourier-transform infrared (FT-IR) measurements were performed in AT-IR mode using a JASCO FT-IR-4600 instrument (Tokyo, Japan). The surface morphology of materials was characterized by scanning electron microscopy (SEM, JEOL JSM-7100, Tokyo, Japan).

2.3. Preparation of TH-FcDA

TH was covalently linked to FcDA in a 2:1 molar ratio using EDC.HCl and HOBT as cross-linking reagents [12], as depicted in Figure 1. FcDA (1 mM) and 2 mmol of EDC.HCl were stirred for 2 h to activate the carboxylic acid (-COOH) groups of ferrocenes for *o*-acylurea formation. Subsequently, 2 mM of HOBT was added to the reaction mixture and stirred vigorously for another 2 h to facilitate ester formation. Then, 2 mmol of TH was introduced, and the reaction mixture was stirred vigorously to promote the reaction of the amine (-NH₂) group in TH with the ester group, resulting in an amide bond formation. The covalently bonded TH-FcDA material was precipitated, washed with ethanol to remove unreacted precursors, and dried in a vacuum oven at 80 °C for 6 h and used for further electrochemical measurements.

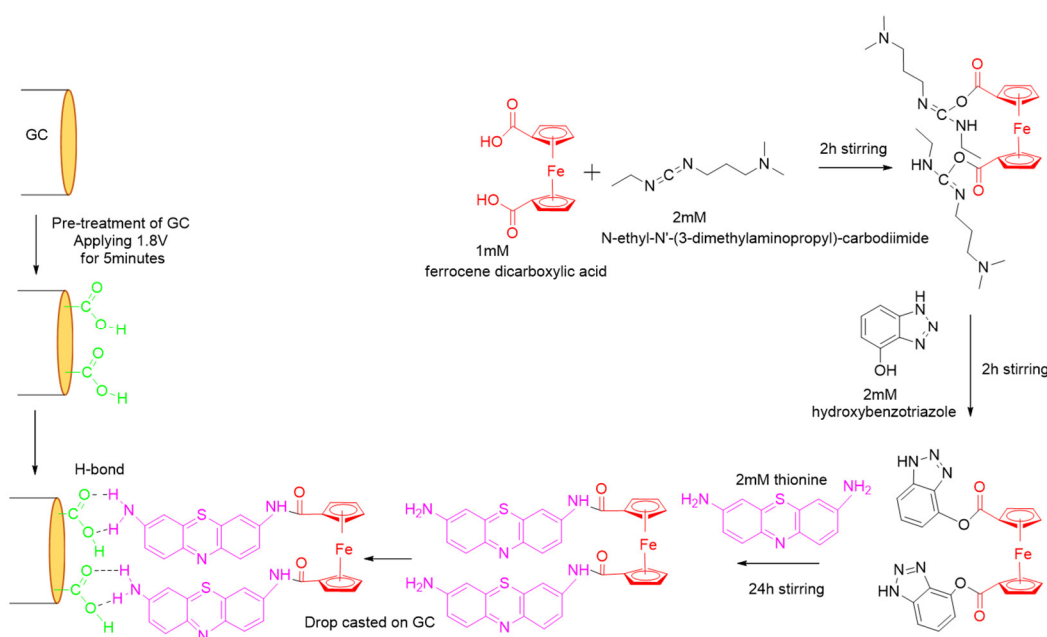


Figure 1. Schematic illustration of the preparation process of the thionine-linked ferrocene dicarboxylic acid-modified GC electrode.

2.4. Modification of GC with TH-FcDA

The GC was surface-cleaned and polished prior to modification. The GC's surface was pre-treated using a chronoamperometric technique previously reported by our group [15,33,34]. The GC was immersed in 0.1 M PBS (pH 7) and subjected to a constant potential of +1.8 V for 300 s. The TH-FcDA solution (5 mg/mL in dimethyl sulfoxide, 3 μ L) was then drop-casted onto the pre-treated GC surface and dried at ambient temperature. The modified electrode (GC/TH-FcDA) was subsequently washed with water to remove any unbonded material and dried under an inert atmosphere.

3. Results and Discussions

3.1. FT-IR and Morphology Studies

The chemical groups of FcDA, TH, and TH-FcDA were characterized via FT-IR, as shown in Figure 2A. The spectra revealed the presence of the -COOH group in FcDA, the NH₂ group in TH, and the amide group in TH-FcDA. The IR bands at 758 and 897 cm^{-1} correspond to the aromatic C-H bending in all three materials. In FcDA, the bands at 1300 and 1672 cm^{-1} confirmed the presence of C-O and C=O stretching vibrations of the -COOH group, respectively [40]. In addition, the IR band at 2926 cm^{-1} corresponds to the C-H stretching in TH [41]. Furthermore, the peaks at 3130 and 3323 cm^{-1} verified the existence of -NH₂ group in TH. Conversely, the C=O stretching vibration shifted to 1606 cm^{-1} with slight broadening owing to the at -CO-NH- bond formation in TH-FcDA. Therefore, the

FT-IR analysis confirmed the formation of the TH-FcDA complex. The morphologies of these materials were analyzed using SEM measurements. The FcDA showed an aggregated and interconnected nanoparticle structure (Figure S1A). In addition, the TH revealed the aggregated nanonetwork-like morphology (Figure S1B). As shown in Figure 2B, the TH-FcDA exhibited a mixed structure with the combination of the interconnected and cluster type of nanoparticle structure and cubic type structure. These structural variations between the materials suggest the formation of TH-FcDA.

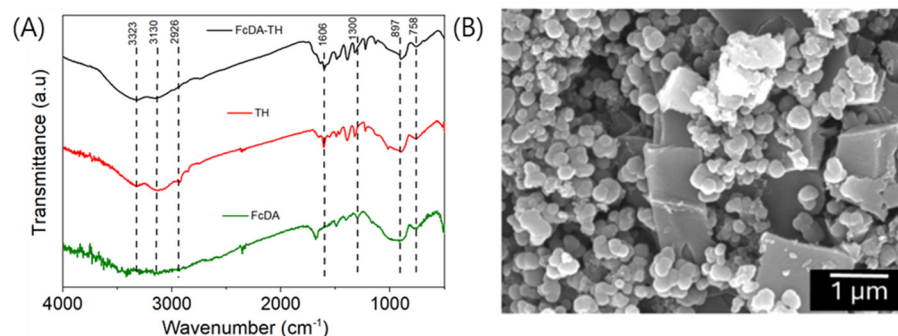


Figure 2. (A) FT-IR spectra of FcDA, TH, and TH-FcDA. (B) SEM images of TH-FcDA.

3.2. Electrochemical Measurements

The cyclic voltammetric (CV) behaviors of **GC**, **GC/FcDA**, **GC/TH**, and **GC/TH–FcDA** were investigated in a 0.1 M PBS at pH 7 with a scan rate of 50 mV/s, and the results are presented in Figure 3. The ferrocene oxidation and reduction peaks (E_{pa} and E_{pc} , respectively) were observed at 0.28 and 0.21 V, respectively, with a ΔE_p of 70 mV for **GC/FcDA**. In comparison, the redox peaks for the formation of TH to leuco-TH were located with E_{pa} and E_{pc} of -0.21 and -0.18 V, respectively, with ΔE_p of 30 mV for **GC/TH**. In the redox complex of the TH-FcDA-modified GC, the ferrocene redox peak shifted negatively, and the current also increased, indicating the TH-mediated redox reaction of FcDA. The TH redox peak current increased in the **GC/TH–FcDA** electrode compared to the **GC/TH** electrode ($\Delta E_p = 10$ mV) with the ΔE_p of 40 mV. This can be attributed to the improved charge transfer properties of the linked moieties resulting from the hydrogen bonding interactions between the $-NH_2$ groups of TH and $-COOH$ functionalities of GC, as schematically presented in Figure 1.

Figure 4A illustrates the CV response of **GC/TH–FcDA** in 0.1 M PBS at pH 7, with DA concentrations varying from 0.3 to 4.5 mM and H_2O_2 concentrations from 3 to 22 μM . The results demonstrate a linear increase in the anodic peak current density (J_{pa}) within the redox potential of FcDA (0.16 V) upon adding DA, with a linear regression equation of J_p (mA/cm^2) = 9.40 [DA] (mM) + 7.01 and a correlation coefficient, $R^2 = 0.9983$ (Figure S2A1). The reduction peak current of TH also increases as the concentration of DA increases in successive CV measurements. This is likely due to the polymerization of DA onto the electrode surface. Additionally, a linear increase in cathodic peak current density (J_{pc}) was observed at -0.2 V with increasing H_2O_2 concentrations, corresponding to a linear regression equation of J_p ($\mu A/cm^2$) = 2.07 [H_2O_2] (μM) + 14.08 ($R^2 = 0.9993$) (Figure S2A2). These demonstrate the low LoDs of 2.77 and 1.37 μM for DA and H_2O_2 , respectively. [12,38] These CV findings suggest that the oxidation of DA to dopamine-o-quinone occurs at FcDA moieties, while the reduction of H_2O_2 to H_2O and $\frac{1}{2}O_2$ occurs at TH moieties (Scheme 1). This was further confirmed using density functional theory (DFT), as detailed in Section 3.5.

Moreover, the different pulse voltammetry (DPV) response of **GC/TH–FcDA** in 0.1 M PBS at pH 7 with DA concentrations ranging from 0.3 to 230 μM and H_2O_2 from 1.5 to 60 μM is shown in Figure 4B. The calibration curve for the electrochemical detection of DA and H_2O_2 using the **GC/TH–FcDA** demonstrated a good linear relationship between the peak currents and the concentrations, spanning 0.3 to 230 μM for DA and 1.5 to 60 μM for H_2O_2 (Figure S2B). The electrode exhibited a linear regression equation of J_{pa}

($\mu\text{A}/\text{cm}^2$) = 0.59 [DA] (μM) + 29.84 with an R^2 of 0.9997 and an estimated sensitivity of $0.59 \mu\text{A}/\mu\text{M}/\text{cm}^2$, indicating the high electrocatalytic activity towards the oxidation of DA at 0.16 V. The LoD was determined to be $0.07 \mu\text{M}$, which is lower than previously reported values for similar electrodes (Table S1A) [12–19]. Furthermore, for H_2O_2 detection, the electrode demonstrated a sensitivity of $0.68 \mu\text{A}/\mu\text{M}/\text{cm}^2$ with a linear regression equation of $J_{\text{pc}} (\mu\text{A}/\text{cm}^2) = 0.68 [\text{H}_2\text{O}_2] + 57.23$ with $R^2 = 0.9996$ and an LoD (S/N = 3) of $0.49 \mu\text{M}$, exceeding earlier findings (Table S1B) [12,21–27].

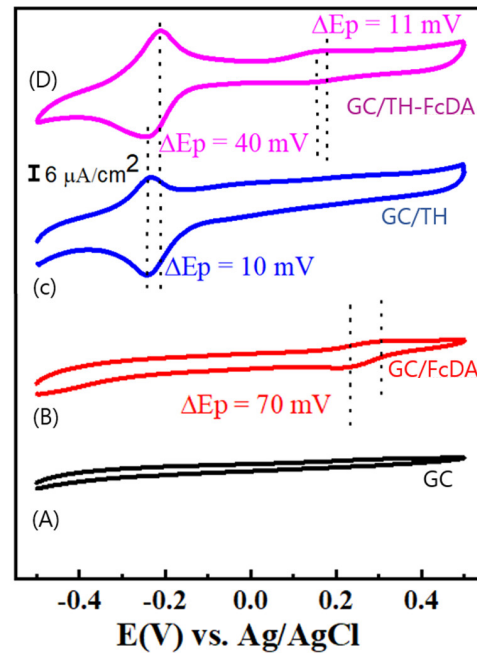


Figure 3. CV behavior of the GC (curve A), GC/FcDA (curve B), GC/TH (curve C), and GC/TH–FcDA (curve D) measured in 0.1 M PBS of pH 7.

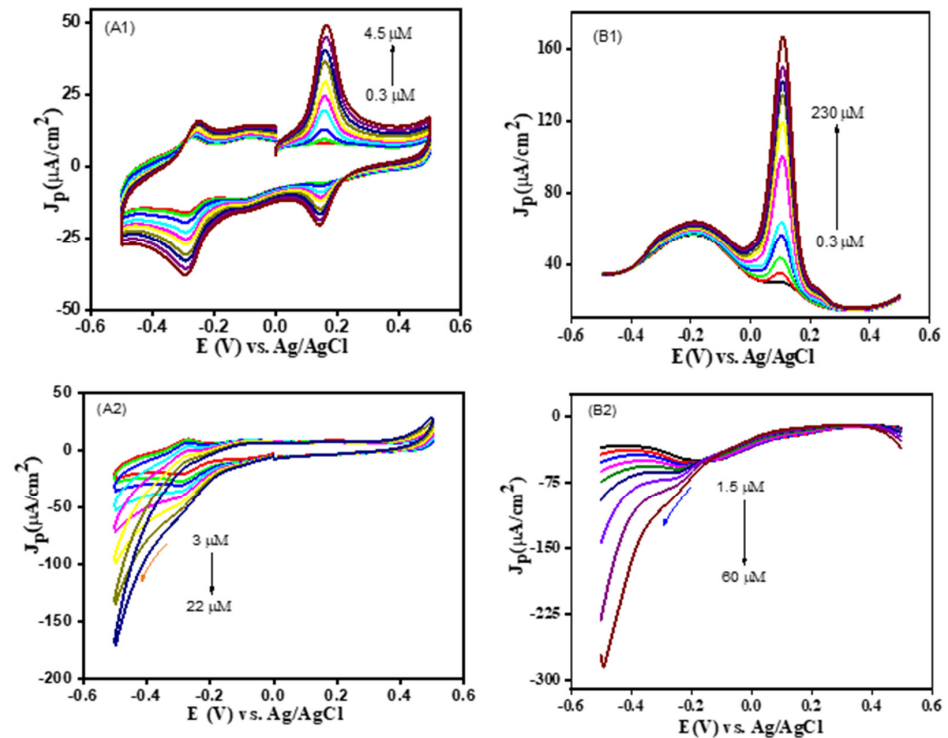


Figure 4. (A) CV and (B) DPV responses of GC/TH–FcDA in 0.1 M PBS (pH 7) at different concentrations of DA (A1 and B1) and H_2O_2 (A2 and B2).

Figure 5(A1,A2) presents the CV response of **GC/TH–FcDA** in 0.1 M PBS at pH 7, featuring both 10 μM of DA and H_2O_2 , with scan rates ranging from 10 to 300 mV/s. The voltammograms reveal that both the J_{pa} and J_{pc} , corresponding to the redox potential of FcDA moieties at 0.15 V, indicative of DA oxidation, increase with the square root of the scan rate. These observations suggest that the DA oxidation process is diffusion-controlled, consistent with findings reported in an earlier study [38]. Similarly, the J_{pc} for the reduction of H_2O_2 increased with the scan rate, which showed linear behavior between J_{pc} and the square root of the scan rate, indicating a diffusion-controlled reduction reaction of H_2O_2 , aligning with previous reports [19].

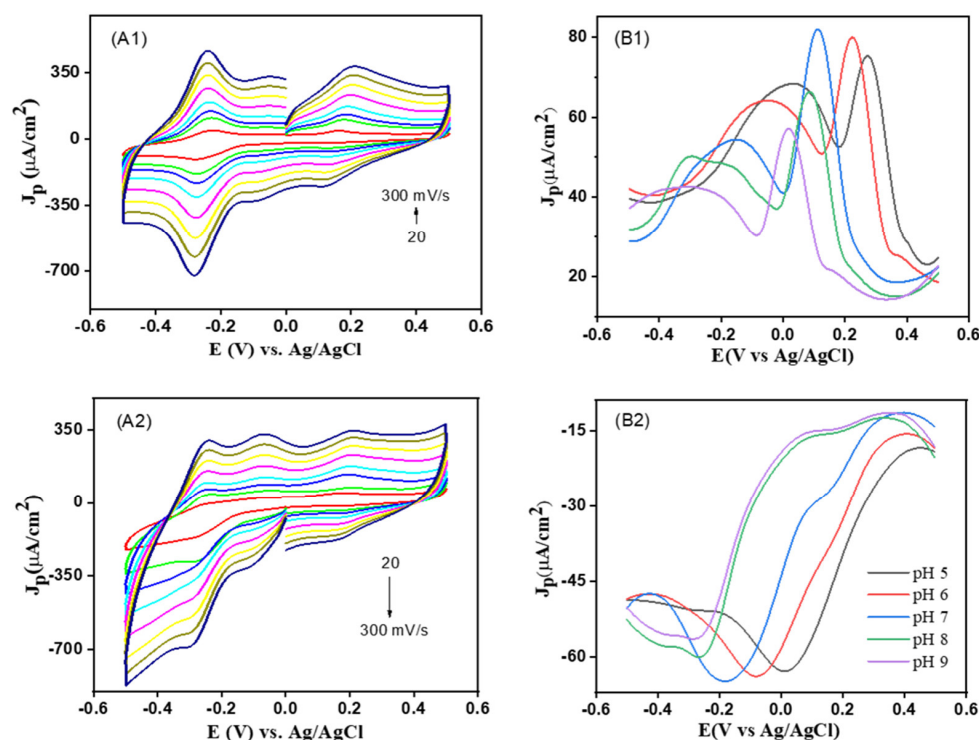


Figure 5. CV response of **GC/TH–FcDA** in 0.1 M PBS (pH 7) in the presence of (A1) 10 μM DA and (A2) 10 μM H_2O_2 at different scan rates (10–300 mV/s). DPV response of **GC/TH–FcDA** in 0.1 M PBS at different pHs (5–9) in the presence of (B1) 10 μM DA and (B2) 10 μM H_2O_2 .

DPV measurements were conducted on **GC/TH–FcDA** to evaluate the influence of supporting electrolyte pH on DA oxidation and H_2O_2 reduction, as depicted in Figure 5(B1,B2). The J_{pa} for DA oxidation increased gradually from pH 5 to 7, followed by a decline from pH 7 to 9 (Figure 5(B1)). The E_{pa} shifted negatively with increasing pH from 5 to 9, described by the linear regression equation $E_{\text{pa}} = -0.065\text{pH} + 0.595$ ($R^2 = 0.995$) (Figure S3A). This result suggests that the stoichiometry for the DA oxidation reaction involved two electrons and two protons [42]. Again, the J_{pc} for H_2O_2 reduction increased with increasing pH from 5 to 7, then decreased from pH 7 to 9 (Figure 5(B2)). The E_{pc} also shifted negatively with rising pH from 5 to 9, quantified by the linear regression equation $E_{\text{pc}} = -0.078\text{pH} + 0.078$ ($R^2 = 0.993$) (Figure S3B). The number of electrons and protons involved in the H_2O_2 reduction was determined to be two [19]. The J_{pa} for DA oxidation and J_{pc} for H_2O_2 reduction reached their maximum at pH 7 (0.1 M PBS), establishing pH 7 (0.1 M PBS) as the optimal supporting electrolyte pH for sensing DA and H_2O_2 .

3.3. Interference Study

The detection of DA (10 μM) and H_2O_2 (10 μM) in the presence of a 100-fold excess of various analytes, including UA, AA, glucose, lysine, cysteine, and catechol, was investigated, and the obtained DPV results are displayed in Figure 6. An additional oxidation

peak at 0.21 V was noted, signifying the oxidation of UA. Importantly, this peak did not interfere with the DA oxidation, attributed to a potential difference of 0.05 V between the oxidation processes of DA and UA. These findings confirm that excess concentrations of other analytes did not affect the detection of DA, and none of the above analytes interferes with the detection of H_2O_2 , demonstrating the good selectivity of the GC/TH–FcDA sensor.

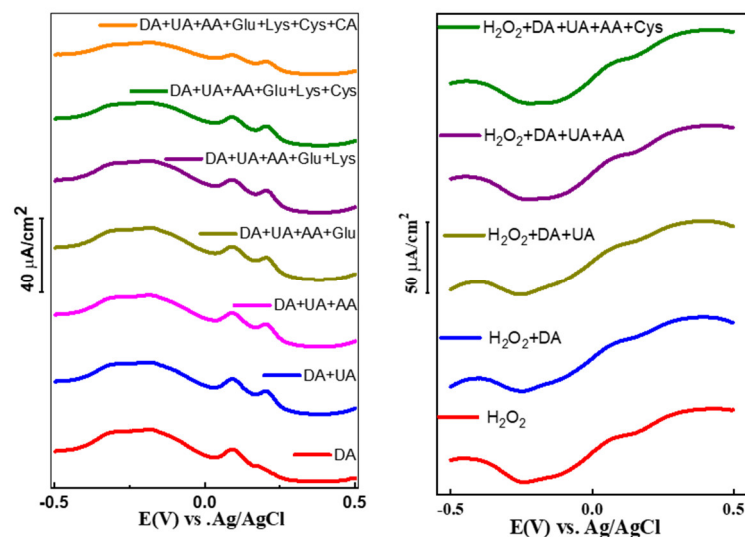


Figure 6. DPV response of 10 μM DA and H_2O_2 with 300 μM of different interference species in 0.1 M PBS pH 7.

3.4. Real-Sample Analysis, Reproducibility, and Stability

To examine the practical applicability of the proposed GC/TH–FcDA sensor, a real-sample analysis was conducted. Human urine samples were pre-treated and stored at 4 °C prior to analysis [38]. H_2O_2 was detected in commercial milk samples. Both DA and H_2O_2 detections were performed using the standard addition method [39]. Five repetitive experiments were conducted for each sample, and recovery measurements were also performed using the standard addition method. The recovery results for DA ranged from 99.8% to 100.08%, while for H_2O_2 , recoveries ranged from 99.2% to 101.0%, as delineated in Table 1. These results substantiate the excellent recovery performance and practical applicability of the developed electrode material.

Table 1. Estimation of DA in diluted human urine samples. Estimation of H_2O_2 in milk samples.

Sample No	Spiked (μM)	Found (μM) *	Recovery (%)	RSD (%)
1	10	9.98 ± 0.02	99.8	0.2
2	50	50.04 ± 0.04	100.08	0.08
3	100	99.89 ± 0.11	99.89	0.11
Sample No	Spiked (μM)	Found (μM) *	Recovery (%)	RSD (%)
1	5	4.96 ± 0.04	99.2	0.8
2	10	10.10 ± 0.10	101	0.99
3	20	20.09 ± 0.09	100.45	0.44

* Average three-replicate measurements.

As depicted in Figure S4, the GC/TH–FcDA demonstrated excellent reproducibility with a relative standard deviation (RSD%) of 0.35% and 0.07%, estimated from 30 consecutive CV scans performed in 10 μM H_2O_2 and DA 0.1 M PBS pH 7, respectively. For a long-term stability study, the GC/TH–FcDA sensor was stored in an airtight container when not in use for 20 days and retained 90% of its initial response. These findings confirm the stability of the electrode and its capacity to resist interference from repeated use cycles.

3.5. Density Functional Theory (DFT) Studies

The geometries and corresponding properties of the computed structures were analyzed using the B3LYP/6-31G (d,p) [43] level of theory with the GAUSSIAN 09 software and visualized with GaussView (5). No imaginary modes were observed in the frequency analysis, confirming that all structures are stationary points. The corresponding geometric coordinates are tabulated in Table S2 [44]. Figure 7 presents the electrostatic potential (ESP) map of TH-FcDA and its interactions with DA and H₂O₂. The DA molecule interacts with TH-FcDA through a potential π - π interaction site on both DA and FcDA molecules. The ESP map of the two materials reveals that the net positive density of TH-FcDA is localized on one side of the FcDA, while the net negative density on DA is oriented towards the aromatic ring, suggesting possible repulsion of DA on the TH side due to the positive charge density at the edges. Additionally, H₂O₂ demonstrates an electrostatic interaction with TH, primarily utilizing the oxygen groups at the positive end of TH.

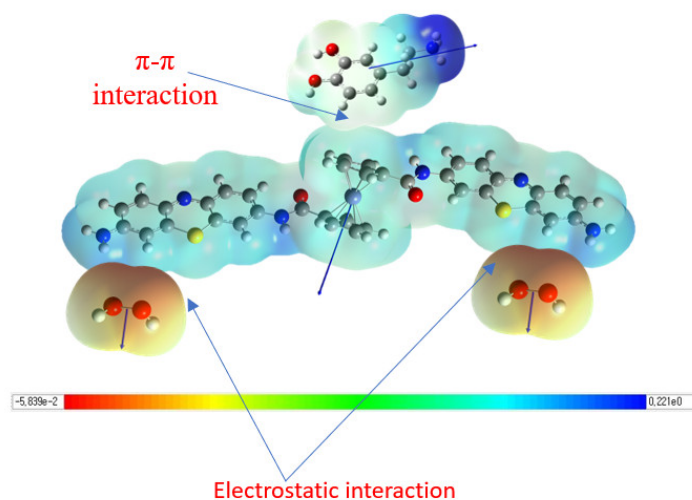


Figure 7. Electrostatic potential (ESP) map for TH-FcDA with DA and H₂O₂.

4. Conclusions

This research successfully developed a highly stable dual redox mediator by covalently linking FcDA and TH onto a GC electrode. The electrochemical investigations elucidated the roles of FcDA and TH moieties in facilitating the oxidation of DA and reduction of H₂O₂, respectively. Carboxylation of the GC surface enhanced the immobilization of the redox mediator, resulting in high stability and a reproducible sensing response under neutral pH conditions. The electrode exhibited a notable sensing performance for DA, with a detection range from 0.3 to 230 μ M, a sensitivity of 0.59 μ A/ μ M/ cm^2 , and a LoD of 0.07 μ M (S/N = 3). Additionally, the electrode enabled effective sensing of H₂O₂, displaying in a range from 1.5 to 60 μ M, with a sensitivity of 0.68 μ A/ μ M/ cm^2 and an LoD of 0.49 μ M (S/N = 3). Notably, the sensor was validated by detecting DA and H₂O₂ in diluted urine and milk samples, demonstrating its potential for practical applications in biosensing.

Supplementary Materials: The following supporting information can be downloaded at: <https://www.mdpi.com/article/10.3390/bios14090448/s1>. Figure S1. SEM images of (A) FcDA, and (B) TH. Figure S2. Linear plot for different concentrations of DA (A1, B1) and H₂O₂ (A2, B2) measured from Figure 4. Figure S3. Linear plot for different pH in the detection of DA (A) and H₂O₂ (B) measured from Figure 5(B1,B2). Figure S4. Reproducibility and Stability of GC/TH–FcDA electrode in the presence of H₂O₂ (A1,A2) and DA (B1,B2). Table S1. A. Comparison of analytical parameters for DA detection at GC/TH–FcDA. B. Comparison of analytical parameters for H₂O₂ detection at GC/TH–FcDA. Table S2. Cartesian coordinates of the molecules.

Author Contributions: Conceptualization, M.P.N. and J.-J.L.; methodology, M.P.N., M.R., J.P., F.K.A., V.P., I.S.A. and B.L.; software, M.P.N. and F.K.A.; formal analysis, M.P.N. and M.R.; validation, M.P.N., M.R., J.P., F.K.A., V.P., I.S.A. and B.L.; writing—original draft preparation, M.P.N.; writing—review and editing, M.M.R., M.R., J.P., F.K.A., V.P., I.S.A., B.L., K.P.K. and J.-J.L.; supervision, K.P.K. and J.-J.L.; project administration, J.-J.L.; funding acquisition, K.P.K. and J.-J.L. All authors have read and agreed to the published version of the manuscript.

Funding: This research was supported by the Korean National Research Foundation, funded by the Ministry of Science, ICT & Future Planning (grant NRF-2021R1A2C2094554).

Institutional Review Board Statement: Not applicable.

Informed Consent Statement: Not applicable.

Data Availability Statement: The original contributions presented in the study are included in the article; further inquiries can be directed to the corresponding authors.

Conflicts of Interest: The authors declare no conflicts of interest.

References

1. Pena-Pereira, F.; Bendicho, C.; Pavlović, D.M.; Martín-Esteban, A.; Díaz-Álvarez, M.; Pan, Y.; Cooper, J.; Yang, Z.; Safarik, I.; Pospiskova, K.; et al. Miniaturized Analytical Methods for Determination of Environmental Contaminants of Emerging Concern—A Review. *Anal. Chim. Acta* **2021**, *1158*, 238108. [[PubMed](#)]
2. Dincer, C.; Bruch, R.; Costa-Rama, E.; Fernández-Abedul, M.T.; Merkoçi, A.; Manz, A.; Urban, G.A.; Güder, F. Disposable Sensors in Diagnostics, Food, and Environmental Monitoring. *Adv. Mater.* **2019**, *31*, e1806739. [[CrossRef](#)] [[PubMed](#)]
3. Armenta, S.; Esteve-Turrillas, F.A.; Garrigues, S.; Guardia, M. de la Smart Materials for Sample Preparation in Bioanalysis: A Green Overview. *Sustain. Chem. Pharm.* **2021**, *21*, 100411. [[CrossRef](#)]
4. Anastas, P.T. Green Chemistry and the Role of Analytical Methodology Development. *Crit. Rev. Anal. Chem.* **1999**, *29*, 167–175. [[CrossRef](#)]
5. Heli, H.; Pishahang, J.; Amiri, H.B. Synthesis of Hexagonal CoAl-Layered Double Hydroxide Nanoshales/Carbon Nanotubes Composite for the Non-Enzymatic Detection of Hydrogen Peroxide. *J. Electroanal. Chem.* **2016**, *768*, 134–144. [[CrossRef](#)]
6. Giorgio, M.; Trinei, M.; Migliaccio, E.; Pelicci, P.G. Hydrogen Peroxide: A Metabolic by-Product or a Common Mediator of Ageing Signals? *Nat. Rev. Mol. Cell Biol.* **2007**, *8*, 722–728. [[CrossRef](#)]
7. Dias, V.; Junn, E.; Mouradian, M.M. The Role of Oxidative Stress in Parkinson's Disease. *J. Parkinsons Dis.* **2013**, *3*, 461–491. [[CrossRef](#)]
8. Drábková, M.; Admiraal, W.; Maršálek, B. Combined Exposure to Hydrogen Peroxide and Light Selective Effects on Cyanobacteria, Green Algae, and Diatoms. *Environ. Sci. Technol.* **2007**, *41*, 309–314. [[CrossRef](#)]
9. Mahbubur Rahman, M.; Liu, D.; Siraj Lopa, N.; Baek, J.-B.; Nam, C.-H.; Lee, J.-J. Effect of the Carboxyl Functional Group at the Edges of Graphene on the Signal Sensitivity of Dopamine Detection. *J. Electroanal. Chem.* **2021**, *898*, 115628. [[CrossRef](#)]
10. Ahammad, A.J.S.; Nath, N.C.D.; Xu, G.-R.; Kim, S.; Lee, J.-J. Interference-Free Determination of Dopamine at the Poly(Thionine)-Modified Glassy Carbon Electrode. *J. Electrochem. Soc.* **2011**, *158*, F106–F110. [[CrossRef](#)]
11. Xi, X.; Tang, W.; Wu, D.; Shen, C.; Ji, W.; Li, J.; Su, Y.; Guo, X.; Liu, R.; Yan, F. All-Carbon Solution-Gated Transistor with Low Operating Voltages for Highly Selective and Stable Dopamine Sensing. *ACS Sens.* **2023**, *8*, 1211–1219. [[CrossRef](#)] [[PubMed](#)]
12. Devendiran, M.; Krishna Kumar, K.; Sriman Narayanan, S. Fabrication of a Novel Ferrocene/Thionin Bimediator Modified Electrode for the Electrochemical Determination of Dopamine and Hydrogen Peroxide. *J. Electroanal. Chem.* **2017**, *802*, 78–88. [[CrossRef](#)]
13. Ognjanović, M.; Stanković, D.M.; Jaćimović, Ž.K.; Kosović-Perutović, M.; Dojčinović, B.; Antić, B. The Effect of Surface-Modifier of Magnetite Nanoparticles on Electrochemical Detection of Dopamine and Heating Efficiency in Magnetic Hyperthermia. *J. Alloys Compd.* **2021**, *884*, 161075. [[CrossRef](#)]
14. Shafi, P.M.; Joseph, N.; Karthik, R.; Shim, J.-J.; Bose, A.C.; Ganesh, V. Lemon Juice-Assisted Synthesis of LaMnO₃ Perovskite Nanoparticles for Electrochemical Detection of Dopamine. *Microchem. J.* **2021**, *164*, 105945. [[CrossRef](#)]
15. Bahrami, E.; Amini, R.; Vardak, S. Electrochemical Detection of Dopamine via Pencil Graphite Electrodes Modified by Cu/Cu₂O Nanoparticles. *J. Alloys Compd.* **2021**, *855*, 157292. [[CrossRef](#)]
16. Anbumannan, V.; Kumar, R.T.R.; Suresh, K. Enhanced Electrochemical Detection of Dopamine by Graphene Oxide/Tungsten Trioxide Nanocomposite. *Mater. Sci. Semicond. Process.* **2021**, *127*, 105696. [[CrossRef](#)]
17. Tian, J.; Wu, W. A Novel Preparation of Water-Dispersed Graphene and Their Application to Electrochemical Detection of Dopamine. *Adv. Powder Technol.* **2021**, *32*, 619–629. [[CrossRef](#)]

18. Mathiarasu, R.R.; Manikandan, A.; Baby, J.N.; Panneerselvam, K.; Subashchandrabose, R.; George, M.; Slimani, Y.; Almessiere, M.A.; Baykal, A. Hexagonal Basalt-like Ceramics $\text{La}_{1-x}\text{Mg}_x\text{TiO}_3$ ($x = 0$ and 0.5) Contrived via Deep Eutectic Solvent for Selective Electrochemical Detection of Dopamine. *Physica B Condens. Matter* **2021**, *615*, 413068. [[CrossRef](#)]
19. Atta, N.F.; Abdel Gawad, S.A.; Galal, A.; Razik, A.A.; El-Gohary, A.R.M. Efficient Electrochemical Sensor for Determination of H_2O_2 in Human Serum Based on Nano Iron-nickel Alloy/Carbon Nanotubes/Ionic Liquid Crystal Composite. *J. Electroanal. Chem.* **2021**, *881*, 114953. [[CrossRef](#)]
20. Sajjan, V.A.; Mohammed, I.; Nemakal, M.; Aralekallu, S.; Kumar, K.H.; Swamy, S.; Sannegowda, L.K. Hemantha Kumar, Sreenivasa Swamy, Lokesh Koodlur Sannegowda, Synthesis and electropolymerization of cobalt tetraaminebenzamidephthalocyanine macrocycle for the amperometric sensing of dopamine. *J. Electroanal. Chem.* **2019**, *838*, 33–40. [[CrossRef](#)]
21. Molodtsova, T.; Gorshenkov, M.; Saliev, A.; Vanyushin, V.; Goncharov, I.; Smirnova, N. One-Step Synthesis of $\gamma\text{-Fe}_2\text{O}_3/\text{Fe}_3\text{O}_4$ Nanocomposite for Sensitive Electrochemical Detection of Hydrogen Peroxide. *Electrochim. Acta* **2021**, *370*, 137723. [[CrossRef](#)]
22. Zhao, J.; Yang, H.; Wu, W.; Shui, Z.; Dong, J.; Wen, L.; Wang, X.; Yang, M.; Hou, C.; Huo, D. Flexible Nickel–Cobalt Double Hydroxides Micro-Nano Arrays for Cellular Secreted Hydrogen Peroxide in-Situ Electrochemical Detection. *Anal. Chim. Acta* **2021**, *1143*, 135–143. [[CrossRef](#)] [[PubMed](#)]
23. Atacan, K.; Özacar, M. Construction of a Non-Enzymatic Electrochemical Sensor Based on $\text{CuO}/\text{g-C}_3\text{N}_4$ Composite for Selective Detection of Hydrogen Peroxide. *Mater. Chem. Phys.* **2021**, *266*, 124527. [[CrossRef](#)]
24. Zhao, F.; Zhou, S.; Zhang, Y. Ultrasensitive Detection of Hydrogen Peroxide Using Bi_2Te_3 Electrochemical Sensors. *ACS Appl. Mater. Interfaces* **2021**, *13*, 4761–4767. [[CrossRef](#)]
25. Liu, X.; Zhang, X.; Zheng, J. One-Pot Fabrication of AuNPs-Prussian Blue-Graphene Oxide Hybrid Nanomaterials for Non-Enzymatic Hydrogen Peroxide Electrochemical Detection. *Microchem. J.* **2021**, *160*, 105595. [[CrossRef](#)]
26. Qiao, X.; Arsalan, M.; Ma, X.; Wang, Y.; Yang, S.; Wang, Y.; Sheng, Q.; Yue, T. A Hybrid of Ultrathin Metal-Organic Framework Sheet and Ultrasmall Copper Nanoparticles for Detection of Hydrogen Peroxide with Enhanced Activity. *Anal. Bioanal. Chem.* **2021**, *413*, 839–851. [[CrossRef](#)]
27. Rashed, M.A.; Harraz, F.A.; Faisal, M.; El-Toni, A.M.; Alsaiari, M.; Al-Assiri, M.S. Gold Nanoparticles Plated Porous Silicon Nanopowder for Nonenzymatic Voltammetric Detection of Hydrogen Peroxide. *Anal. Biochem.* **2021**, *615*, 114065. [[CrossRef](#)]
28. Ghanbari, K.; Bonyadi, S. Modified Glassy Carbon Electrode with Polypyrrole Nanocomposite for the Simultaneous Determination of Ascorbic Acid, Dopamine, Uric Acid, and Folic Acid. *J. Electrochem. Sci. Technol.* **2020**, *11*, 68–83. [[CrossRef](#)]
29. Peng, J.; Li, X.; Liu, Y.; Zhuge, W.; Zhang, C.; Huang, Y. Photoelectrochemical Sensor Based on Zinc Phthalocyanine Semiconducting Polymer Dots for Ultrasensitive Detection of Dopamine. *Sens. Actuators B Chem.* **2022**, *360*, 131619. [[CrossRef](#)]
30. Sai Iswarya Bakavaty, T.; Gurunathan, K. Graphene-Wrapped WO_3/Mo Derivatives for the Simultaneous Electrochemical Detection of Dopamine and Uric Acid. *Mater. Sci. Eng. B* **2024**, *299*, 116967. [[CrossRef](#)]
31. Barber, R.; Davis, J.; Papakonstantinou, P. Stable Chitosan and Prussian Blue-Coated Laser-Induced Graphene Skin Sensor for the Electrochemical Detection of Hydrogen Peroxide in Sweat. *ACS Appl. Nano Mater.* **2023**, *6*, 10290–10302. [[CrossRef](#)]
32. Rahman, M.M.; Lee, J.J. Electrochemical Dopamine Sensors Based on Graphene. *J. Electrochem. Sci. Technol.* **2019**, *10*, 185–195.
33. Nankya, R.; Opar, D.O.; Jung, H. Mesoporous Graphene-Modified Electrode for Independent and Selective Detection of Dopamine in the Presence of High Concentration of Ascorbic Acid. *Bull. Korean Chem. Soc.* **2020**, *41*, 170–175. [[CrossRef](#)]
34. Wang, Z.; Zhang, L.; Tian, Y. A Durable Non-Enzymatic Electrochemical Sensor for Monitoring H_2O_2 in Rat Brain Microdialysates Based on One-Step Fabrication of Hydrogels. *Analyst* **2015**, *140*, 3788–3793. [[CrossRef](#)]
35. Mahbubur Rahman, M.; Lee, J.-J. Sensitivity Control of Dopamine Detection by Conducting Poly(Thionine). *Electrochem. Commun.* **2021**, *125*, 107005. [[CrossRef](#)]
36. Rahman, M.M.; Lopa, N.S.; Kim, K.; Lee, J.-J. Selective Detection of L-Tyrosine in the Presence of Ascorbic Acid, Dopamine, and Uric Acid at Poly(Thionine)-Modified Glassy Carbon Electrode. *J. Electroanal. Chem.* **2015**, *754*, 87–93. [[CrossRef](#)]
37. Sree, V.G.; Sohn, J.I.; Im, H. Pre-Anodized Graphite Pencil Electrode Coated with a Poly(Thionine) Film for Simultaneous Sensing of 3-Nitrophenol and 4-Nitrophenol in Environmental Water Samples. *Sensors* **2022**, *22*, 1151. [[CrossRef](#)]
38. Rahman, M.M.; Lopa, N.S.; Ju, M.J.; Lee, J.-J. Highly Sensitive and Simultaneous Detection of Dopamine and Uric Acid at Graphene Nanoplatelet-Modified Fluorine-Doped Tin Oxide Electrode in the Presence of Ascorbic Acid. *J. Electroanal. Chem.* **2017**, *792*, 54–60. [[CrossRef](#)]
39. Sangeetha, N.S.; Narayanan, S.S. A Novel Bimediator Amperometric Sensor for Electrocatalytic Oxidation of Gallic Acid and Reduction of Hydrogen Peroxide. *Anal. Chim. Acta* **2014**, *828*, 34–45. [[CrossRef](#)]
40. Kumar, T.N.; Sivabalan, S.; Chandrasekaran, N.; Phani, K.L.N. Ferrocene-functionalized polydopamine as a novel redox matrix for H_2O_2 oxidation. *J. Mater. Chem. B* **2014**, *2*, 6081–6088. [[CrossRef](#)]
41. Thenmozhi, K.; Narayanan, S.S. Carbon paste electrode with covalently immobilized thionine for electrochemical sensing of hydrogen peroxide. *IOP Conf. Ser. Mater. Sci. Eng.* **2017**, *263*, 022031. [[CrossRef](#)]
42. Manikandan, P.N.; Dharuman, V. Electrochemical Simultaneous Sensing of Melatonin, Dopamine and Acetaminophen at Platinum Doped and Decorated Alpha Iron Oxide. *Electroanalysis* **2017**, *29*, 1524–1531. [[CrossRef](#)]

43. Stephens, P.J.; Devlin, F.J.; Ashvar, C.S.; Bak, K.L.; Taylor, P.R.; Frisch, M.J. *Comparison of Local, Nonlocal, and Hybrid Density Functionals Using Vibrational Absorption and Circular Dichroism Spectroscopy*; American Chemical Society: Washington, DC, USA, 1996; pp. 105–113.
44. Frisch, M.J.; Trucks, G.W.; Schlegel, H.B.; Scuseria, G.E.; Robb, M.A.; Cheeseman, J.R.; Scalmani, G.; Barone, V.; Mennucci, B.; Petersson, G.A.; et al. *Gaussian 09, Revision B.01*; Gaussian, Inc.: Wallingford, CT, USA, 2013.

Disclaimer/Publisher's Note: The statements, opinions and data contained in all publications are solely those of the individual author(s) and contributor(s) and not of MDPI and/or the editor(s). MDPI and/or the editor(s) disclaim responsibility for any injury to people or property resulting from any ideas, methods, instructions or products referred to in the content.